

NUMERICAL MODELLING OF FREE SURFACE FLOWS IN METALLURGICAL VESSELS

Peter LIOVIC¹, Murray RUDMAN² and Jong-Leng LIOW¹

¹ GK Williams Cooperative Research Centre for Extractive Metallurgy
Department of Chemical Engineering
The University of Melbourne, Parkville, Victoria, AUSTRALIA

² CSIRO Division of Building, Construction and Engineering
Highett, Victoria, AUSTRALIA

ABSTRACT

A numerical model is presented for the transient solution to multi-fluid problems defined in complex 2-D rectangular and cylindrical geometries. The model, using a piecewise linear volume tracking scheme to track interfaces, maintains sharp interfaces and captures fine-scale flow phenomena such as fragmentation and coalescence. Two applications are presented. The first studied the entrainment of matte in slag during slag skimming operations. Flow fields from the simulation showed pressure gradients caused by the light liquid accelerating down over the weir resulted in the heavier liquid being rotated upwards and over the weir. The second studied splash as a result of top-submerged gas injection. The model showed the phenomena of bubble formation, bubble rise, and splash drop formation and re-coalescence with the bath in detail. Data of engineering interest such as pressure traces and time-averaged flow fields were generated, facilitating assessment of splash behaviour for given gas injection conditions.

Keywords: volume tracking gas injection

NOMENCLATURE

t	time
\mathbf{U}	velocity
P	pressure
τ	stress tensor
\mathbf{g}	acceleration due to gravity
\mathbf{S}	surface force due to surface tension
ρ	density
μ	viscosity
C	color function
σ	surface tension
\mathbf{n}	interfacial normal vector
κ	interfacial curvature

INTRODUCTION

Tools capable of predicting metallurgical free surface flows are invaluable in realising operational improvements in metallurgical unit operations. Two examples of interest in the area of pyrometallurgy include the skimming operation in Peirce-Smith converters and top-submerged gas injection in Ausmelt furnaces.

Peirce-Smith converters are “skimmed” to remove all the overlying slag phase from the vessel. This is a pouring operation carried out by rotating the converter. Valuable matte is entrained in the flow of the slag out of the converter during this pouring. Minimising matte losses while maximising slag removal, referred to as selective withdrawal, is the target of the slag skimming operation from Peirce-Smith converters.

The essence of Ausmelt bath smelting technology (Floyd, 1996) is the top injection of reagent gases through lances submerged beneath the free surface of the molten slag bath. The slag that is thrown into the gas space above the bath by the intense agitation induced by gas injection is referred to as “splash”. This cascade of slag above the bath peaks in the post-combustion zone, shown in Figure 1. In the post-combustion zone of the Ausmelt furnace, additional oxygen is added to combust carbon monoxide generated in the smelting reaction zone, incomplete fuel combustion products, or coal volatiles. The slag cascade absorbs heat generated in the post-combustion zone, resulting in energy recovery to the bath. Studies in pilot and commercial plant operations indicate energy recovery to the bath from reactions in the post-combustion zone is between 30 and 60 percent (Sofra and Mounsey, 1999).

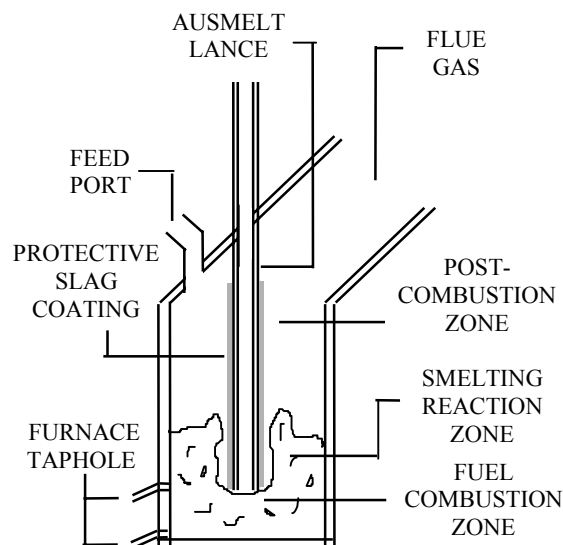


Figure 1: Schematic diagram of Ausmelt Furnace

The fluid flow patterns in the metallurgical unit operations described present complex free surface flow problems. These flows are highly transient in nature and can involve massive amounts of fragmentation and coalescence of fluid bodies. Accurate CFD modelling of such free surface flows should capture the transient nature of these flows, and faithfully represent free surfaces, within a geometrically complex flow domain. A number of different methods, distinguished by the way the position of the interface over time is located, have been developed to simulate free surface flows. These methods, whether they are tracking (Lagrangian) or capturing (Eulerian) methods, are commonly referred to as interface tracking. Rudman (1997) and Kothe (1998) provide brief overviews and assessments of these different methods. For the flow problems presented, methods for interface tracking should effectively represent phenomena such as the fragmentation and coalescence of fluid bodies. Interface tracking should also allow for the incorporation of other physics (Kothe, 1998), should be easy to implement, and should allow multiple fluid layers to be modelled simultaneously. Based on the requirements outlined, *volume tracking* methods are the most attractive option for a numerical code to simulate complex free surface flows. Effective multi-fluid volume tracking methods are therefore at the core of the numerical method presented.

NUMERICAL MODEL

Equations of Motion

The numerical model directly solves the equations governing incompressible isothermal multi-fluid flows

$$\nabla \cdot \mathbf{U} = 0 \quad (1)$$

$$\frac{\partial \mathbf{U}}{\partial t} + \nabla \cdot \mathbf{U}\mathbf{U} = -\frac{1}{\rho} \nabla P + \frac{1}{\rho} \nabla \cdot \boldsymbol{\tau} + \mathbf{g} + \frac{1}{\rho} \mathbf{S} \quad (2)$$

Volume tracking methods represent multiple immiscible fluids with a characteristic (“color”) function C

$$C = \begin{cases} 1 & \text{in cells full of a particular fluid} \\ 0 & \text{in cells devoid of that particular fluid} \end{cases} \quad (3)$$

For n fluid species there are $n-1$ color functions. The location of the interface is not explicitly tracked, but is instead captured by the distribution of C , since C takes the values $0 \leq C \leq 1$ on interfaces. Species mass conservation requires C to fulfil the equation

$$\frac{\partial C}{\partial t} + \nabla \cdot (\mathbf{U}C) = 0 \quad (4)$$

Bulk properties such as density and viscosity are recovered as weighted averages based on C .

Solution Algorithm

The coupled equations of motion for incompressible isothermal multi-fluid flow are solved using a two-step projection. The solution algorithm for advancing the solution of the flow field from time n to $n+1$ is as follows:

1. Determine the fluid topology by updating all color functions:

$$C^{n+1} = C^n - \delta t \nabla \cdot (\mathbf{U}C) \quad (5)$$

2. Compute new density and viscosity distributions based on C^{n+1} .

3. Make an initial estimate of the (non-solenoidal) velocity field (\mathbf{U}^*), based on the solution at time n

$$\mathbf{U}^* = \mathbf{U}^n + \delta t \begin{bmatrix} -\nabla \cdot (\mathbf{U}\mathbf{U})^n - \frac{1}{\rho^n} \nabla P \\ + \frac{1}{\rho^n} \nabla \cdot \boldsymbol{\tau}^n + \mathbf{g} + \frac{1}{\rho^n} \mathbf{S}^n \end{bmatrix} \quad (6)$$

4. Solve the Poisson equation for the pressure correction (δP) to ensure continuity is satisfied

$$\nabla \cdot \left(\frac{1}{\rho^n} \nabla \delta P \right) = \frac{1}{\delta t} \nabla \cdot \mathbf{U}^* \quad (7)$$

5. Update the velocity and pressure fields to time $n+1$

$$\mathbf{U}^{n+1} = \mathbf{U}^* - \frac{\delta t}{\rho^n} \nabla \delta P \quad (8)$$

$$P^{n+1} = P^n + \delta P \quad (9)$$

The solution algorithm as described is first order in time. Euler's improved time-stepping scheme is implemented to improve temporal accuracy to second order. Steps (3) to (5) are done twice - firstly with a half time-step, and secondly with a full time-step, but using values of \mathbf{U} , P , ρ and μ from the half time-step solution.

Discretisation of the Flow Domain

Spatial discretisations of the equations in the solution algorithm are based on a uniform MAC mesh (Welch *et al.*, 1966). Scalar variables such as pressure and C are located at cell centres, while velocities are located at the centre of and normal to cell edges. Finite difference discretisations of all terms in the equations of the solution algorithm have been used. Also used is a stairstep representation of flow obstacles, where whole cells are ignored if they lie within an obstacle. The discretisations used are second order accurate in space as well as in time.

Volume Tracking

Step 1 of the solution algorithm is carried out using volume tracking, based on the piecewise linear interface calculation (PLIC) method of Youngs (1982). The method is second order accurate and maintains very sharp interfaces. In the method, line segments are used to reconstruct fluid-fluid interfaces within interface cells. The orientation of the interfacial line segment is estimated using weighted averaging based on C in surrounding cells. Fluxes of individual species across cell edges in a given timestep are based on this interface reconstruction and cell edge flux velocities. Direction splitting is implemented to apply this procedure to two-dimensional flows; the application of horizontal and vertical fluxes first in the C update is alternated to avoid introducing systematic error into the solution. The implemented method is applicable to both 2D rectangular and axisymmetric geometries.

Surface Force Modelling

Surface tension is readily accommodated in the numerical model by the use of C , using ideas introduced in the CSF method of Brackbill *et al.* (1992). In the CSF method, surface tension is modelled as a body force applied in a thin transition region representing the interface, in which the distribution of C varies smoothly. In the limit of infinitesimal grid spacing, the transition region vanishes

and the distribution of C is discontinuous as in physical reality. The surface force in the transition region is

$$\mathbf{S} = \sigma \kappa \hat{\mathbf{n}} \quad (10)$$

where the curvature κ is also a function of the unit interfacial normal. The original CSF method used finite difference approximations of normals and curvature using C . Rudman (1998) found the grid-based noise introduced by such finite difference approximations to be inherently noisy, and developed a method which instead used convolution with a smoothing kernel (and its derivatives) to define normals and curvature. This method, combined with a kernel with good smoothing properties for small smoothing lengths, was shown by Rudman (1998) to be a big improvement on the original CSF method. Most importantly, introduced errors are kept small, which means surface tension can be modelled accurately without fear of noise destroying the solution in time.

MULTI-LIQUID FLOW OVER A WEIR

Understanding the flow of liquid layers over a weir is important in understanding the entrainment of matte in slag during skimming from Peirce-Smith converters. Multi-liquid flow over a weir is a good validation problem for the numerical model, for which quality experimental data has been obtained (Assaad *et al.*, 1998).

In the multi-liquid flow over a weir problem, a barrier retains a fluid body with a light layer over a denser liquid layer. At time $t = 0$, the barrier is removed, allowing liquid to fall over the weir under gravity. Figure 2 shows the initialisation of the problem. The right and bottom walls of the computational flow domain coincide with walls in the experimental rig, and were therefore simulated as no-slip boundaries. The weir is an internal flow obstacle with no-slip boundaries. There is no ceiling on the experimental rig, and the left wall of the rig is very far away from the weir. Gas dynamics in the air far away from the liquid are relatively unimportant, so the left and top boundaries were simulated as free-slip boundaries.

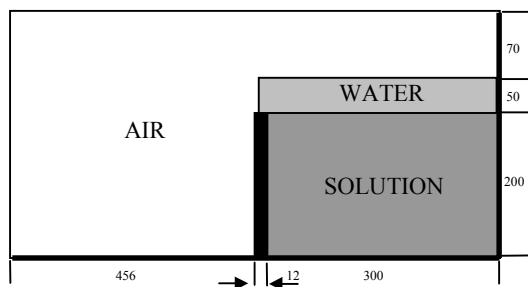


Figure 2 : Schematic diagram of simulation set-up.

For this problem, computational meshes up to resolution 256×128 were used. Surface tension was not considered important in this problem, and was neglected. Table 1 below lists relevant bulk properties for the light liquid (water) and the heavy liquid (salt solution).

Fluid	Density (kg/m ³)	Viscosity (cP)
Light liquid	997	0.9997
Heavy liquid	1047	1.15

Table 1: Physical property data.

Figure 3 compares interfacial profiles from the 256×128 mesh simulation with experimental video images. As can be seen, the results compare favourably. Figure 4 compares measurements of the height of the fluid-fluid interfaces in a line adjacent with the right weir edge.

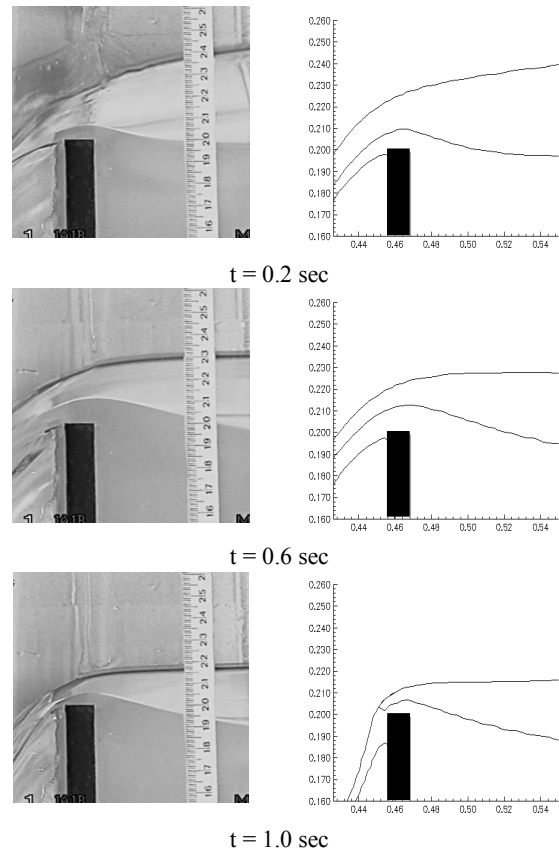


Figure 3: Comparison of (a) numerical and (b) experimental interfacial profiles.

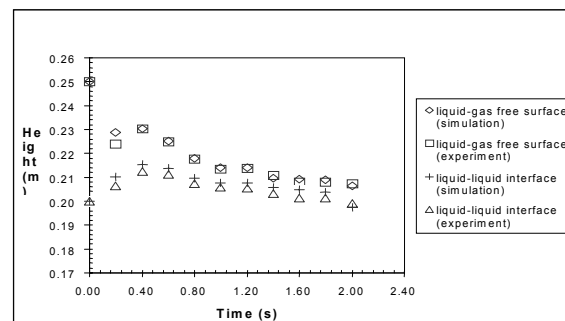


Figure 4: Interfacial positions above the bottom wall at the right wall of the weir.

As seen, the differences between simulation and experiment are small. Another means of assessing the accuracy of the simulation is by comparing, after the flow of heavy liquid over the weir has ceased, the entrainment

$$Entrainment = V2/V1 \quad (11)$$

$V2$ and $V1$ are the volumes of heavy and light liquid respectively that fell over the weir. The results are shown in Table 2, using results from 128×64 and 192×96 meshes.

	Liq./liq. interface (mm)	Entrainment	Error
Experiment	181.6	0.7011	
128×64 mesh	180.7	0.7595	8.3 %
192×96 mesh	181.1	0.7331	4.6 %

Table 2: Entrainment results.

Error is smaller in the case of the finer mesh, indicating some degree of grid dependence. For both simulations, the error in the entrainment is low, and the error in the interface height relative to the total change in the interface is even lower. This indicates that grid dependence is small, with the numerical method capable of generating meaningful solutions on relatively coarse meshes. The accuracy of the results verifies the schemes used in the numerical model, and validates the model for problems with multiple fluids and flow obstacles.

A validated numerical model means simulation results can yield insights into the physics of flow problems that are difficult to obtain experimentally. The interfacial profiles in Figure 3 initially show the lighter liquid falling over the weir under gravity, and heavier liquid adjacent to the weir flowing to the top of the weir. The heavier liquid reaches above the top of the weir, and is entrained in the flow of the top liquid over the weir. Entrainment subsides after $t = 1.0$ sec, after which a back-wave is initiated in the liquid. Figure 5, which shows velocity vectors and dynamic pressure contours from the simulation at $t = 0.5$ sec, provides insight into the mechanism of entrainment.

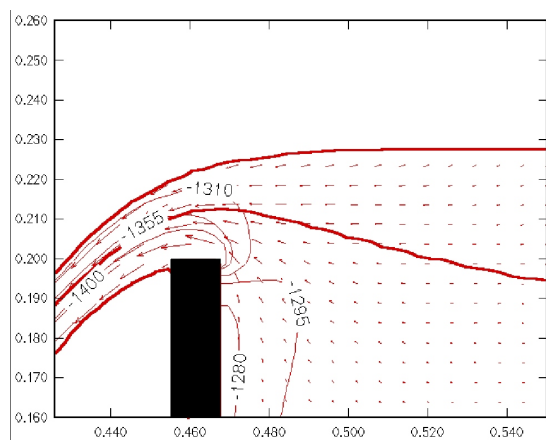


Figure 5: Interfacial profiles, velocity vectors and pressure contours for the flow field at $t = 0.5$ sec.

The liquids falling over the weir are accelerated under gravity. The increased velocity of liquid in this area is accompanied by a local drop in pressure. The result, as shown by the contours in Figure 5, is a pressure gradient between liquid falling over the top of the weir and heavy liquid behind and adjacent to the weir. This pressure gradient is sufficient to lift the heavy liquid adjacent to the weir above the top of the weir, upon which it is entrained in the light liquid falling under gravity over the weir.

TOP-SUBMERGED GAS INJECTION

As a first step in studying post-combustion in an Ausmelt furnace, top-submerged gas injection in a bench-scale cylindrical vessel was investigated. Injection of air

downwards through the lance was commenced at time $t = 0$. The problem initialisation is illustrated in Figure 6.

Top-submerged gas injection was simulated as a 2D axisymmetric problem. All rigid walls were simulated as being no-slip walls. Inside the lance at the top of the vessel was set as a constant inflow boundary. An outflow boundary was established as an annulus in the top of the vessel around the outside of the lance. Outflow velocities were not set to be constant, but instead computed by Equation (8). Based on the method outlined by Sani and Gresho (1994), the net inflow based on the intermediate flow field was computed by Equation (6). This net inflow was used to compute the boundary condition on the pressure correction - a non-homogeneous Neumann boundary condition. The gradient in the pressure correction across the boundary set the velocities at outflow boundaries, ensuring global volume conservation.

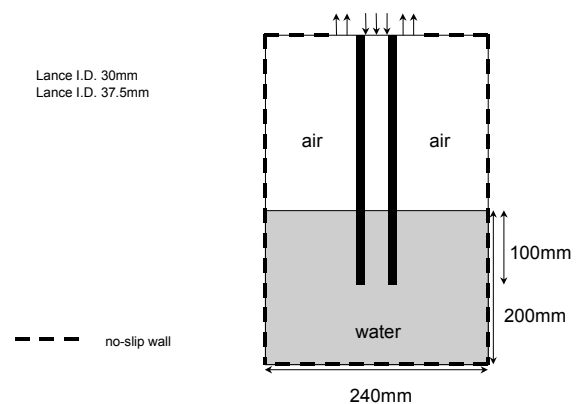


Figure 6 : Schematic diagram of simulation set-up.

For these simulations, a mesh resolutions of 64×128 (vessel height taken as 400mm) was used. Simulations were performed for two different bath liquids – water, and a 95 percent glycerol solution. Both of these liquids are transparent and relatively hazard-free. In experimental studies of the top-submerged gas injection, this means techniques such as video, laser doppler anemometry (LDA) and particle image velocimetry (PIV) can be used to good effect. The relevant physical properties used for both liquids are given in Table 3 below. The 95 percent glycerol solution was chosen for simulations as a high viscosity alternative to water, enabling assessment of the effect of viscosity on phenomena resulting from gas injection. The effect of viscosity on the flow resulting from top-submerged gas injection is of interest because of the high viscosity of metallurgical slags.

Bath Liquid	95 percent glycerol soln.	Water
Density (kg/m^3)	1250	575
Viscosity (cP)	997	1.005
Surface tension (dynes/cm)	63.91	73.6

Table 3: Liquids in top-submerged gas injection studies.

The first case simulated used the glycerol solution, with an average gas inlet velocity of 1.0 m/s. Figure 7 shows

frames of the fluid topology in the cylindrical vessel at selected times after the commencement of gas injection. In this case, splashing was minimal.

Figure 8(a) shows the pressure signal recorded during the simulation at a point near the top of the lance, with sampling at 1 kHz. The signal is clearly periodic, indicating that the prevailing bubbling regime for this given gas flow rate is constant frequency bubbling. The Fourier Transform of the pressure signal (Figure 8(b)) clearly shows the bubbling frequency to be 5 Hz, a frequency commonly seen in industrial studies of bubbling in metallurgical vessels.

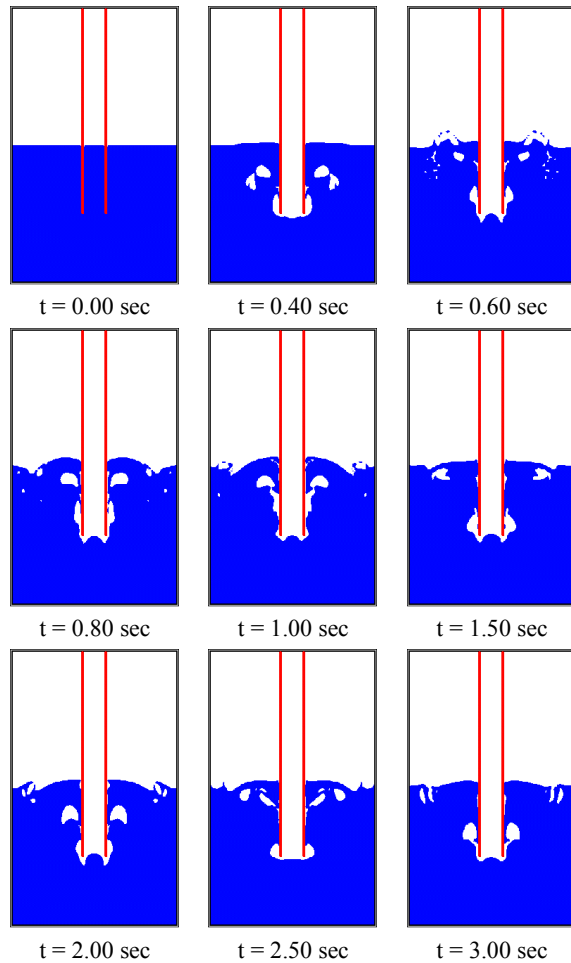
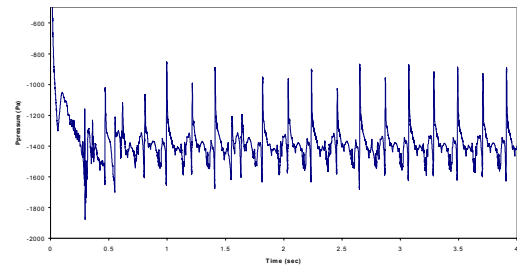
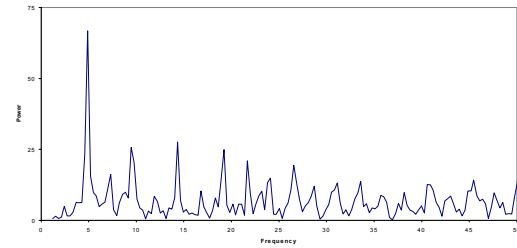


Figure 7: Frames of simulation results at selected times for injection into 95 percent glycerol solution at 1.0 m/s.

Figure 9, showing the average void fraction throughout the computational flow domain for the given injection case, is a powerful summary of the simulation. The trajectory of bubbles that detach from the lance tip is clear – initially adjacent to the lance and then moving outwards from the lance at the free surface under bulk bath flow, before bursting. Splashing and free surface distortions are highly suppressed by the high liquid viscosity, as seen by comparing the mean free surface location in Figure 9 with the quiescent free surface seen initially in Figure 7. The high viscosity of the glycerol solution damps out bulk bath motion, a result of this apparent from both Figures 7 and 9 being the lack of back-penetration of liquid up the lance.



(a)



(b)

Figure 8: (a) Pressure signal recorded inside the lance, for injection into 95 percent glycerol solution at 1.0 m/s, and (b) the Fourier Transform of the pressure signal.

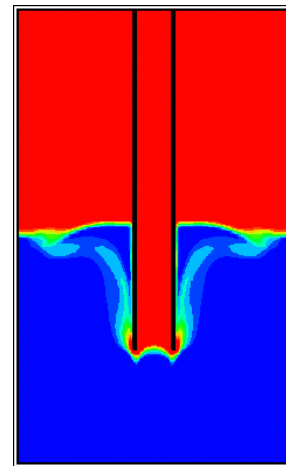


Figure 9: Average void fraction within cylindrical vessel, for injection into 95 percent glycerol solution at 1.0 m/s.

The second case simulated used water as the bath liquid, with no change in geometry and again an average gas inlet velocity of 1.0 m/s. Figure 10 shows frames of the fluid topology in the cylindrical vessel at selected times after gas injection is started. Figure 11 shows the pressure signal at the top of the inside of the lance.

In this case, splashing is significant. The comparison between the frames in Figure 7 and the frames in Figure 10 shows how strongly increased bath liquid viscosity suppresses free surface deformations and splash formation. Water ligaments and splash droplets are thrown well above the quiescent free surface height all across the vessel, although the highest ejections are in close proximity to the lance. Unlike in the case of the 95 percent glycerol solution, the bubbling behavior is greatly influenced by bulk bath flow. This is seen by the frequent

back-penetration of liquid, often reaching far up the inside of the lance. A result of this is that the flow for the case of water is less regularly periodic than for the 95 percent glycerol solution, as borne out by the signal in Figure 11.

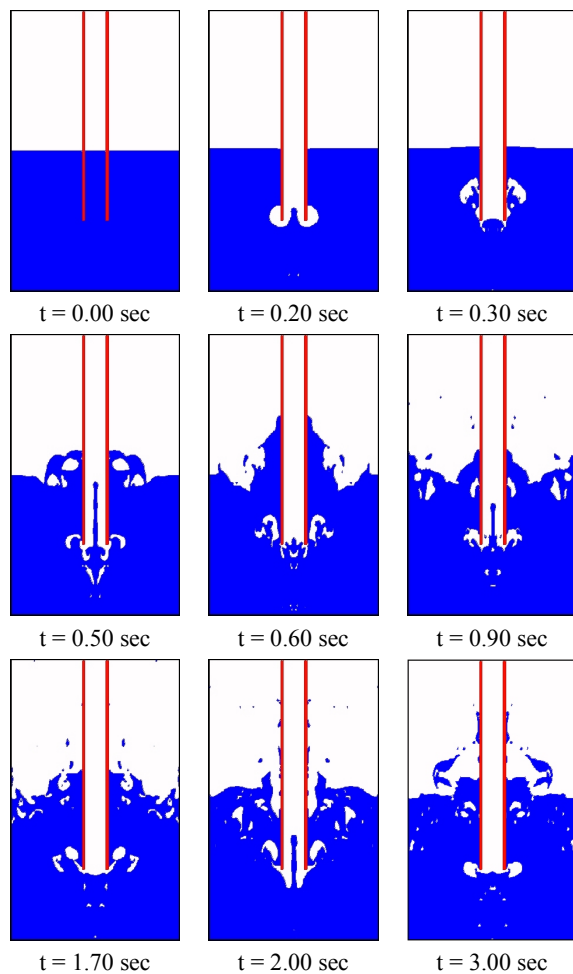


Figure 10: Frames of simulation results at selected times for injection into water at 1.0 m/s.

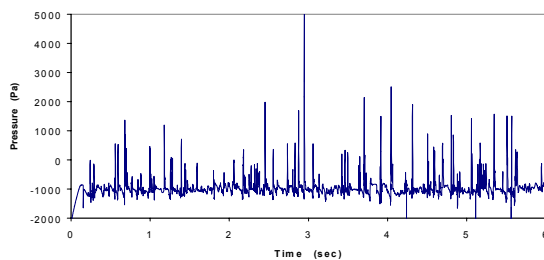


Figure 11: Pressure signal recorded inside the lance, for injection into water at 1.0 m/s.

CONCLUSION

A numerical model has been developed to simulate complex free surface flows in metallurgical vessels. The model uses volume tracking with piecewise linear interface reconstructions to ensure fluid-fluid interfaces are kept sharp. The numerical model accurately solves the three-fluid problem of multi-liquid flow over a weir. Numerical outputs also yield the entrainment mechanism

in this problem. The numerical model can also tackle the complex problem of top-submerged gas injection. Apart from instantaneous flow fields, the numerical model can generate useful engineering data over time. Viscosity was found to have a strong effect on gas injection. Where liquid viscosity is high, both liquid motions are damped, both suppressing splash and moderating bulk bath flow such that constant frequency bubbling prevails. For low viscosity liquids, bath motion is much more chaotic, with significant splash formation. Bath liquid motions result in back-penetration up the lance, resulting in deviation away from constant frequency bubbling behaviour.

ACKNOWLEDGEMENTS

Financial support for this work was provided by the Australian Minerals Industry Research Association (AMIRA) using facilities provided by the G.K. Williams Cooperative Research Centre for Extractive Metallurgy, a joint venture between CSIRO Minerals and the Department of Chemical Engineering, The University of Melbourne. Special thanks to George Assaad, GKW-CRC, for the multi-liquid flow over a weir results, and to Dr. Joseph Sofra, Ausmelt Limited, for his valuable insights into Ausmelt bath smelting technology.

REFERENCES

- ASSAAD, G.E., LIOW, J.-L., and GRAY, N.B., (1998), "Slag-Metal Flow over a Weir", *Proceedings of the Thirteenth Australasian Fluid Mechanics Conference*, (Eds. M.C. Thompson, K. Hourigan), Monash University, Clayton, pp. 445-448.
- RACKBILL, J.U., KOTHE, D.B. and ZEMACH, C., (1992) "A Continuum Method for Modelling Surface Tension", *Journal of Computational Physics*, Vol. 100, pp. 335-354.
- FLOYD, J.M., (1996), "The Third Decade of Top Submerged Lance Technology", *The Howard Worner International Symposium on Injection in Pyrometallurgy*, (Eds. M. Nilmani, T. Lehner), TMS, pp. 417-429.
- KOTHE, D.B., (1998) "Perspective on Eulerian Finite Volume Methods for Incompressible Interfacial Flows", *Free Surface Flows*, (Eds. H.C. Kuhlmann, H-J Rath), Springer-Verlag, pp. 267-331.
- RUDMAN, M., (1997), "A Volume-Tracking Method for Incompressible Multi-Fluid Flows with Large Density Variations", *Int. J. Num. Meth. Fluids*, pp. 671-691.
- SAAD, Y., (1996), *Iterative Methods for Sparse Linear Systems*, PWS.
- SOFRA, J. and MOUNSEY, E., (1999), "Recent Pilot Scale Development of the Ausiron Direct Ironmaking Process", *SCANMET I – 1st International Conference on Process Development in Iron and Steelmaking*, MEFOS, pp. 301-324.
- YOUNGS, D.L., (1982), "Time-Dependent Multi-Material Flow with Large Fluid Distortion", *Numerical Methods for Fluid Dynamics*, (Eds. K.W. Morton and M.J. Baines), Academic, pp. 273-285.